## K – Ar dating:

Two – branched decay:

only about 1/10

$$^{40}K \begin{cases} \rightarrow {}^{40}Ar & \lambda_\beta = 5.81 \cdot 10^{-11}\, yr^{-1} \quad (\tau_{1/2} = 11.9 \text{ b.y.}) \\ \rightarrow {}^{40}Ca & \lambda_{ec} = 4.96 \cdot 10^{-10}\, yr^{-1} \quad (\tau_{1/2} = 1.4 \text{ b.y.}) \end{cases}$$

about 9/10

Half life

$$\tau_{1/2}^{total} = \frac{0.693}{\lambda_\beta + \lambda_{ec}}$$

$$= 1.25 \text{ b.y.}$$

Useful for old igneous rocks.

Daughter $^{40}Ar$ — noble gas — easily lost from melt or upon reheating — provides age of crystallization

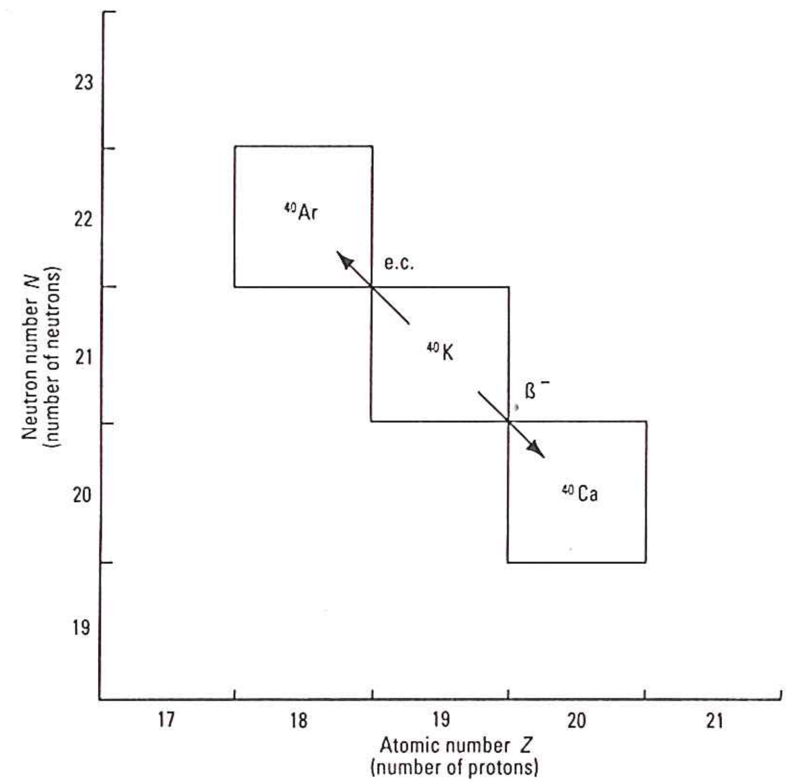


*Fig.* 3.3. $^{40}K$ decays by $\beta^-$ emission to $^{40}Ca$ and by electron capture to $^{40}Ar$ in a ratio of 8.5 to 1. Only the decay to Ar is used for radiometric dating.

$$\boxed{\begin{aligned} t &= \frac{1}{\lambda_\beta + \lambda_{ec}} \ln\left( \frac{^{40}Ar}{^{40}K} \frac{\lambda_\beta + \lambda_{ec}}{\lambda_{ec}} + 1 \right) \\ &= 1.804 \cdot 10^9 \ln\left( 9.54 \frac{^{40}Ar}{^{40}K} + 1 \right) \text{ years} \end{aligned}}$$

Present-day abundance — same in all rocks

$$\left(\frac{{}^{40}K}{{}^{39}K}\right)_{today} = \frac{1}{7970}$$

## $^{40}Ar - {}^{39}Ar$ method:

Irradiate sample in nuclear fission reactor

$$^{39}K + n \rightarrow {}^{39}Ar + p^+ + e^-$$

93% in rocks

$$\boxed{t = 1.804 \cdot 10^9 \ln\left(J \frac{{}^{40}Ar}{{}^{39}Ar} + 1\right)}$$

measure ratio with mass spectrometer

Determine $J$ using a similarly irradiated sample of known age.

$$J = \frac{e^{\lambda t_{known}} - 1}{\left({}^{40}Ar/{}^{39}Ar\right)_{known}}$$

Step-heating: determine plateau age

- mineral separates or whole rock
- provides evidence of any re-heating

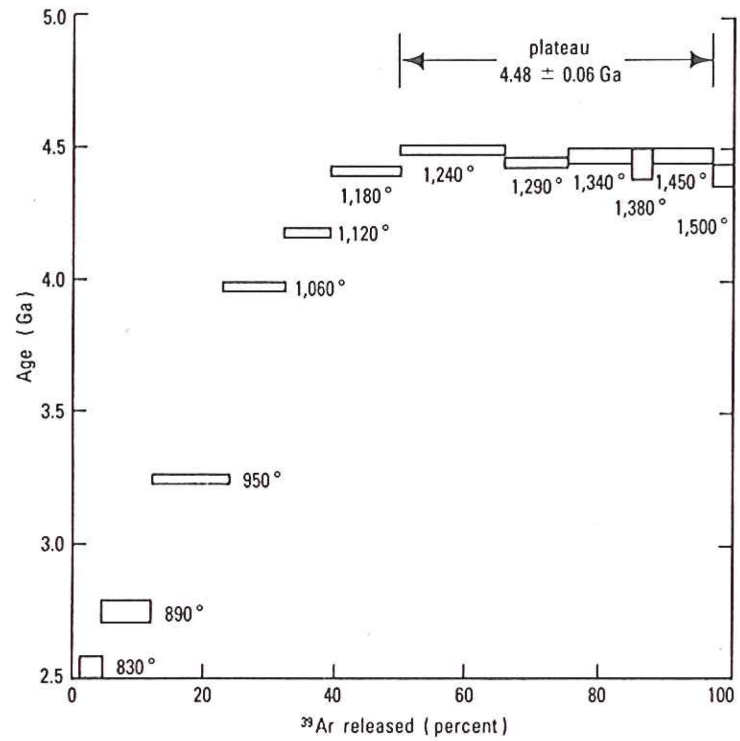


*Fig. 3.12.* $^{40}Ar/^{39}Ar$ age spectrum for the meteorite Menow, which lost 25% of its Ar at about 2.5 Ga. The temperature at which each gas increment was released is shown in degrees Celsius. (After Turner, Enright, and Cadogan, 1978.)

Instead of the amounts of K and Ar being measured in separate experiments by different methods, as is done in the conventional K–Ar method, the exact ratio of daughter to parent in the sample is determined by measuring the ratio of $^{40}Ar$ to $^{39}Ar$ in one experiment. Corrections must be made for atmospheric Ar and for certain interfering Ar isotopes produced by unwanted neutron reactions with Ca and other K isotopes, but these corrections can be made quite precisely and for old rocks are usually very small or negligible. This method of measuring all of the Ar in a sample in one experiment generally gives an age comparable to one determined by the conventional K–Ar method (including necessary corrections, described by Brereton, 1970, Dalrymple and Lanphere, 1971, Dalrymple et al., 1981, Faure, 1986, and McDougall and Harrison, 1988).[14]

An age calculation from $^{40}Ar/^{39}Ar$ data is done with an equation

$$t = 1.804 \times 10^9 \log_e\left(J \frac{^{40}\mathrm{Ar}}{^{39}\mathrm{Ar}} + 1\right)$$

where $J$ is a constant that includes a factor for the fraction of $^{39}K$ converted to $^{39}Ar$ during the irradiation. $J$ is determined for each irradiation by irradiating a sample of known age, a monitor, alongside the unknown sample and using Equation 3.20 to calculate $J$ for the monitor. The value of $J$ for the monitor applies to the unknown sample as well because both the monitor and the unknown sample receive the same dose of neutrons.

# Rb – Sr method

$^{87}Rb \rightarrow {}^{87}Sr + \beta^-$

beta decay

$\tau_{1/2} = 49$ b.y.

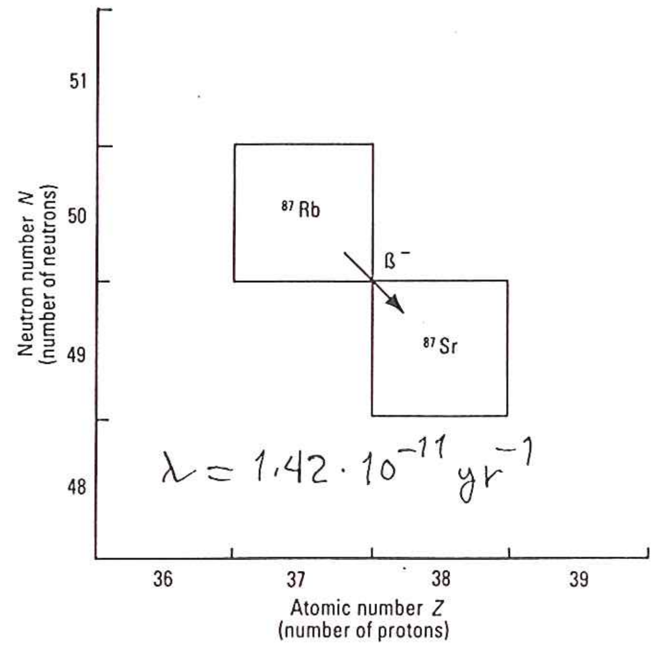


$\lambda = 1.42 \cdot 10^{-11}\ yr^{-1}$

Fig. 3.4. $^{87}$Rb decays to $^{87}$Sr by $\beta^-$ emission.

About one in every 1600 K atoms in a typical silicate mineral is substituted for by Rb

$K/Rb \approx 1600$

Ionic radii are comparable

K – 1.33 Å

Rb — 1.5 Å

Daughter $^{87}Sr$ remains tightly bound in crystal lattice

Initial daughter problem ($D_0 \neq 0$) solved using isochron method

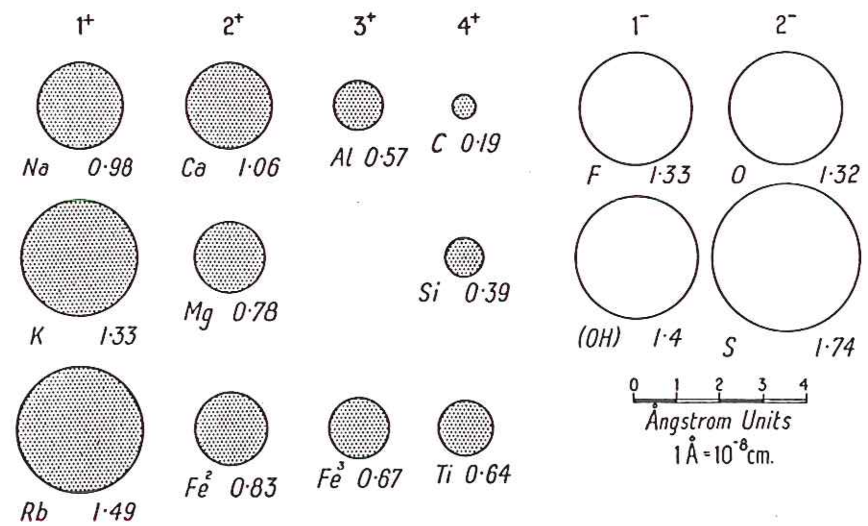


Fig. 49. Relative sizes of some positive ions (*cations*) and negative ions (*anions*) in crystals. The figure at the head of each column refers to the ionic charge or valency. The effective ionic radius of the field of influence of each ion within a crystal, conventionally regarded as spherical, is given in ångstroms.

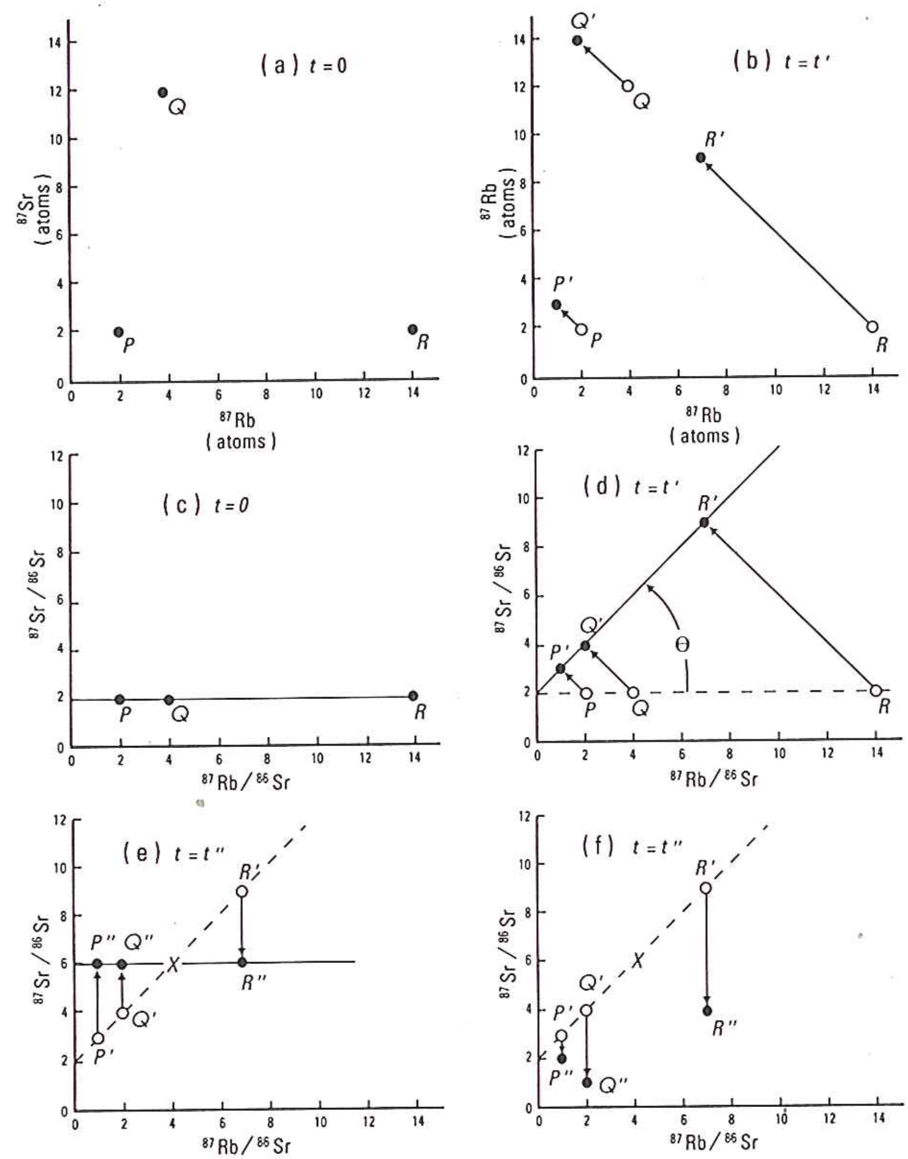


*Fig. 3.9.* (a) Plot of $^{87}$Rb vs $^{87}$Sr for three minerals, $P$, $Q$, and $R$, from a hypothetical rock of zero age. (b) Because of the decay of $^{87}$Rb, points $P$, $Q$, and $R$ move along trajectories of decreasing $^{87}$Rb and increasing $^{87}$Sr to $P'$, $Q'$, and $R'$ after passage of time $t'$. The amount of movement is proportional to the $^{87}$Rb content of the minerals, but this type of plot gives no information about the age of the rock. (c) The same data at $t = 0$ but normalized to $^{86}$Sr. (d) After time $t'$ has passed, the points still fall on a line, an isochron, whose slope is a function of age. (e) Complete resetting of the Rb–Sr clock at time $t''$ moves the points to a new "zero-age" isochron. The composition of the total rock is indicated by $x$. (f) Partial resetting, in this example due to loss of $^{87}$Sr, results in the points scattering.

TABLE 3.1

*Principal Parent and Daughter Isotopes Used to Determine the Ages of Rocks and Minerals*

| Parent isotope (radioactive) | Daughter isotope (stable) | Half-life (Ma) | Decay constant ($yr^{-1}$) |
|---|---|---|---|
| $^{40}$K | $^{40}$Ar[a] | 1,250 | $5.81 \times 10^{-11}$ |
| $^{87}$Rb | $^{87}$Sr | 48,800 | $1.42 \times 10^{-11}$ |
| $^{147}$Sm | $^{143}$Nd | 106,000 | $6.54 \times 10^{-12}$ |
| $^{176}$Lu | $^{176}$Hf | 35,900 | $1.93 \times 10^{-11}$ |
| $^{187}$Re | $^{187}$Os | 43,000 | $1.612 \times 10^{-11}$ |
| $^{232}$Th | $^{208}$Pb | 14,000 | $4.948 \times 10^{-11}$ |
| $^{235}$U | $^{207}$Pb | 704 | $9.8485 \times 10^{-10}$ |
| $^{238}$U | $^{206}$Pb | 4,470 | $1.55125 \times 10^{-10}$ |

[a] $^{40}$K also decays to $^{40}$Ca, for which the decay constant is $4.962 \times 10^{-10}$ $yr^{-1}$, but that decay is not used for dating. The half-life is for the parent isotope and so includes both decays.

## Isochron method

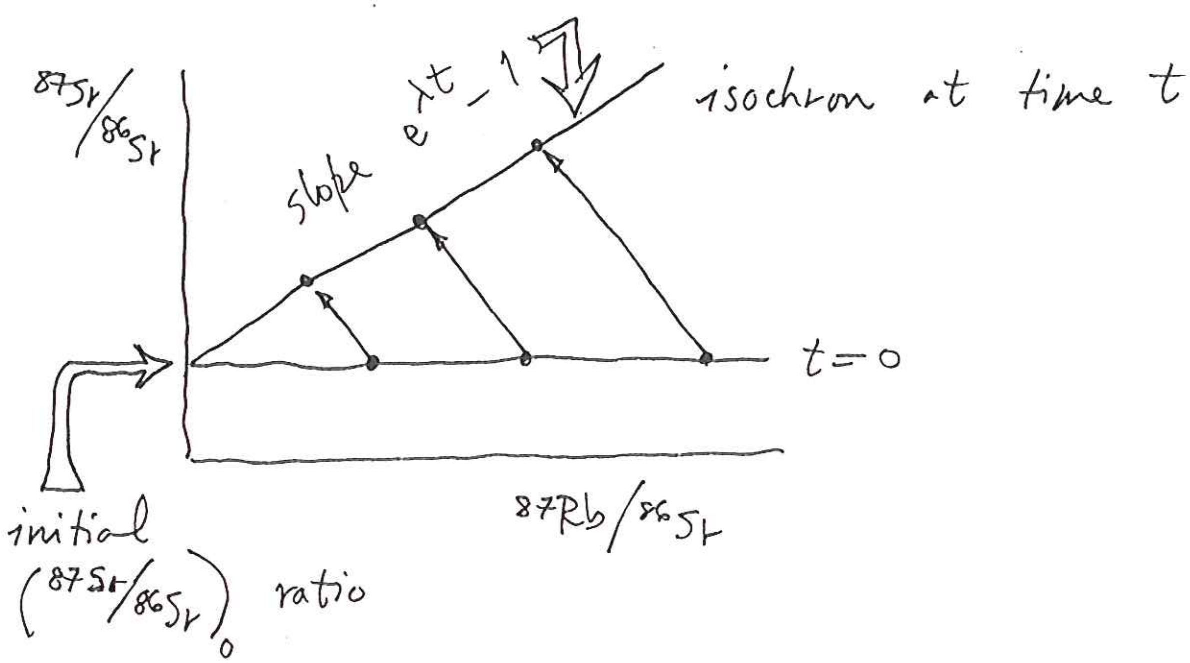


$$^{87}Sr = (^{87}Sr)_0 + (e^{\lambda t}-1)\,^{87}Rb$$

Normalize by dividing by $^{86}Sr$

$$\boxed{\left(\frac{^{87}Sr}{^{86}Sr}\right) = \left(\frac{^{87}Sr}{^{86}Sr}\right)_0 + (e^{\lambda t}-1)\left(\frac{^{87}Rb}{^{86}Sr}\right)}$$

Isochron – straight line of form $y = mx + b$

Intercept $b$ : $\left(\frac{^{87}Sr}{^{86}Sr}\right)_0 \approx 0.7$ initial Sr isotope ratio

at time $t=0$

Slope $m$ : gives age

$$\boxed{\text{slope} = e^{\lambda t}-1}$$

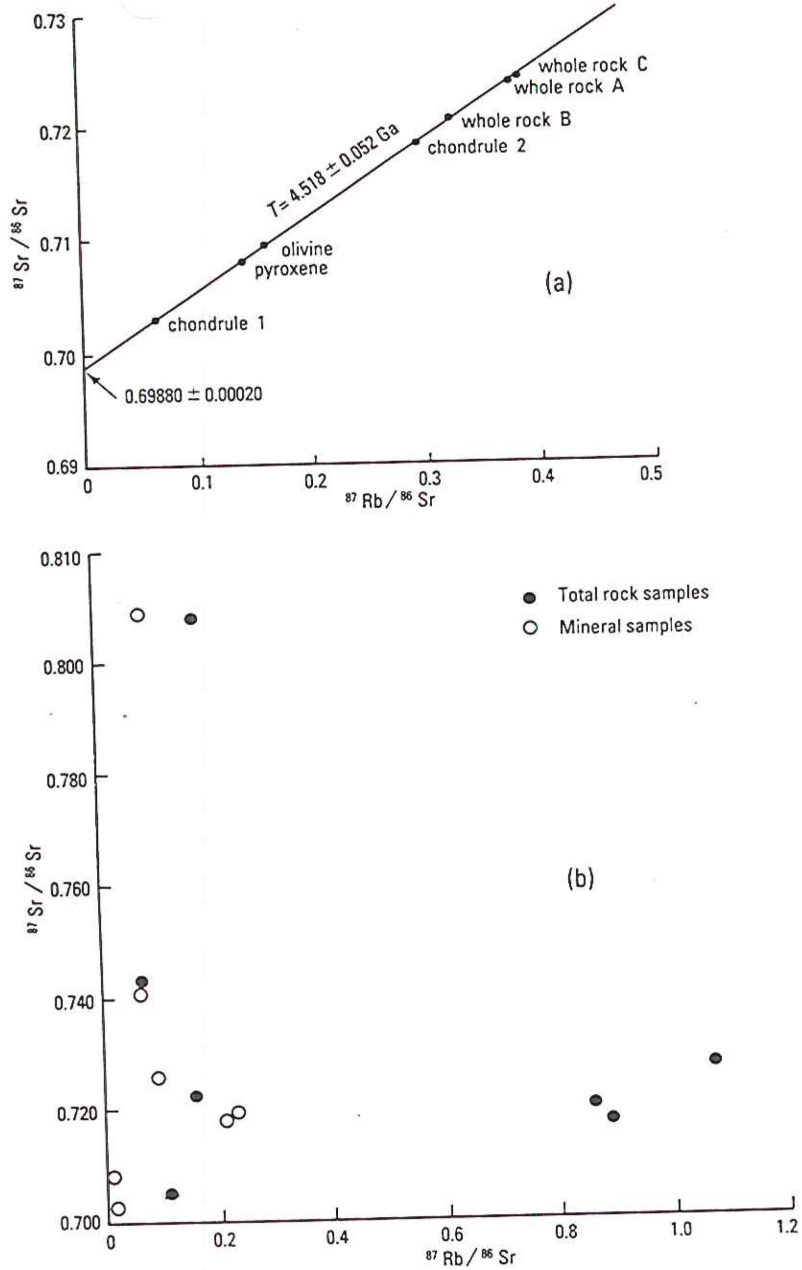


*Fig. 3.10.* (a) A mineral and whole-rock Rb–Sr isochron for the chondrite meteorite Tieschitz. (After Minster and Allègre, 1979a.) (b) Plot of Rb–Sr data for samples from igneous dikes and sills that intrude the Pahrump Group of the Panamint Mountains, California. The scatter of data shows clearly that these samples have been open systems, did not form at the same time, or both. Regardless, the ages of these rocks cannot be determined from these data.

TABLE 3.2

*Natural Abundances of the Isotopes Used in Radiometric Dating*

| Isotope | Abundance (%) |
|---|---|
| $^{39}K$ | 93.26 |
| $^{40}K$ | 0.0117 |
| $^{41}K$ | 6.73 |
| $^{85}Rb$ | 72.17 |
| $^{87}Rb$ | 27.83 |
| $^{144}Sm$ | 3.0 |
| $^{147}Sm$ | 14.9 |
| $^{148}Sm$ | 11.2 |
| $^{149}Sm$ | 13.8 |
| $^{150}Sm$ | 7.4 |
| $^{152}Sm$ | 26.8 |
| $^{154}Sm$ | 22.9 |
| $^{175}Lu$ | 97.4 |
| $^{176}Lu$ | 2.6 |
| $^{185}Re$ | 37.40 |
| $^{187}Re$ | 62.6 |
| $^{232}Th$ | 100.0 |
| $^{234}U$ | 0.0057 |
| $^{235}U$ | 0.72 |
| $^{238}U$ | 99.27 |

| Isotope | Abundance (%) |
|---|---|
| $^{36}Ar$ | 0.337 |
| $^{38}Ar$ | 0.063 |
| $^{40}Ar$ | 99.60 |
| $^{84}Sr$ | 0.56 |
| $^{86}Sr$ | 9.87 |
| $^{87}Sr$ | 7.04 |
| $^{88}Sr$ | 82.53 |
| $^{142}Nd$ | 27.3 |
| $^{143}Nd$ | 12.3 |
| $^{144}Nd$ | 23.8 |
| $^{145}Nd$ | 8.3 |
| $^{146}Nd$ | 17.1 |
| $^{148}Nd$ | 5.7 |
| $^{150}Nd$ | 5.6 |
| $^{174}Hf$ | 0.17 |
| $^{176}Hf$ | 5.2 |
| $^{177}Hf$ | 18.5 |
| $^{178}Hf$ | 27.2 |
| $^{179}Hf$ | 13.8 |
| $^{180}Hf$ | 35.1 |
| $^{184}Os$ | 0.02 |
| $^{186}Os$ | 1.6 |
| $^{187}Os$ | 1.6 |
| $^{188}Os$ | 13.3 |
| $^{189}Os$ | 16.1 |
| $^{190}Os$ | 26.4 |
| $^{192}Os$ | 41.0 |
| $^{204}Pb$ | 1.4 |
| $^{206}Pb$ | 25.2 |
| $^{207}Pb$ | 21.7 |
| $^{208}Pb$ | 51.7 |

NOTE: Abundances are for the Earth's crust except for argon, which is for the atmosphere. The isotopic abundances for those elements that include a daughter isotope vary because of decay of the corresponding parent isotope. The isotope pairs used in radiometric dating are indicated by arrows.

SOURCES: Lederer, Holland, and Perlman, 1967; Faure, 1986.

TABLE 3.3

*Parameters of the Common Radiometric Age-Diagnostic Diagrams*

| Diagram name | Ordinate ($y$ axis) | Abscissa ($x$ axis) |
|---|---|---|
| Rb–Sr isochron | $^{87}Sr/^{86}Sr$ | $^{87}Rb/^{86}Sr$ |
| Sm–Nd isochron | $^{143}Nd/^{144}Nd$ | $^{147}Sm/^{144}Nd$ |
| Lu–Hf isochron | $^{176}Hf/^{177}Hf$ | $^{176}Lu/^{177}Hf$ |
| Re–Os isochron | $^{187}Os/^{186}Os$ | $^{187}Re/^{186}Os$ |
| $^{40}Ar/^{39}Ar$ age spectrum | age or $^{40}Ar/^{39}Ar$ | $^{39}Ar$ released |
| $^{40}Ar/^{39}$ isochron | $^{40}Ar/^{36}Ar$ | $^{39}Ar/^{36}Ar$ |
| Pb–Pb isochron | $^{207}Pb/^{204}Pb$ | $^{206}Pb/^{204}Pb$ |
| U–Pb concordia | $^{206}Pb/^{238}U$ | $^{207}Pb/^{235}U$ |

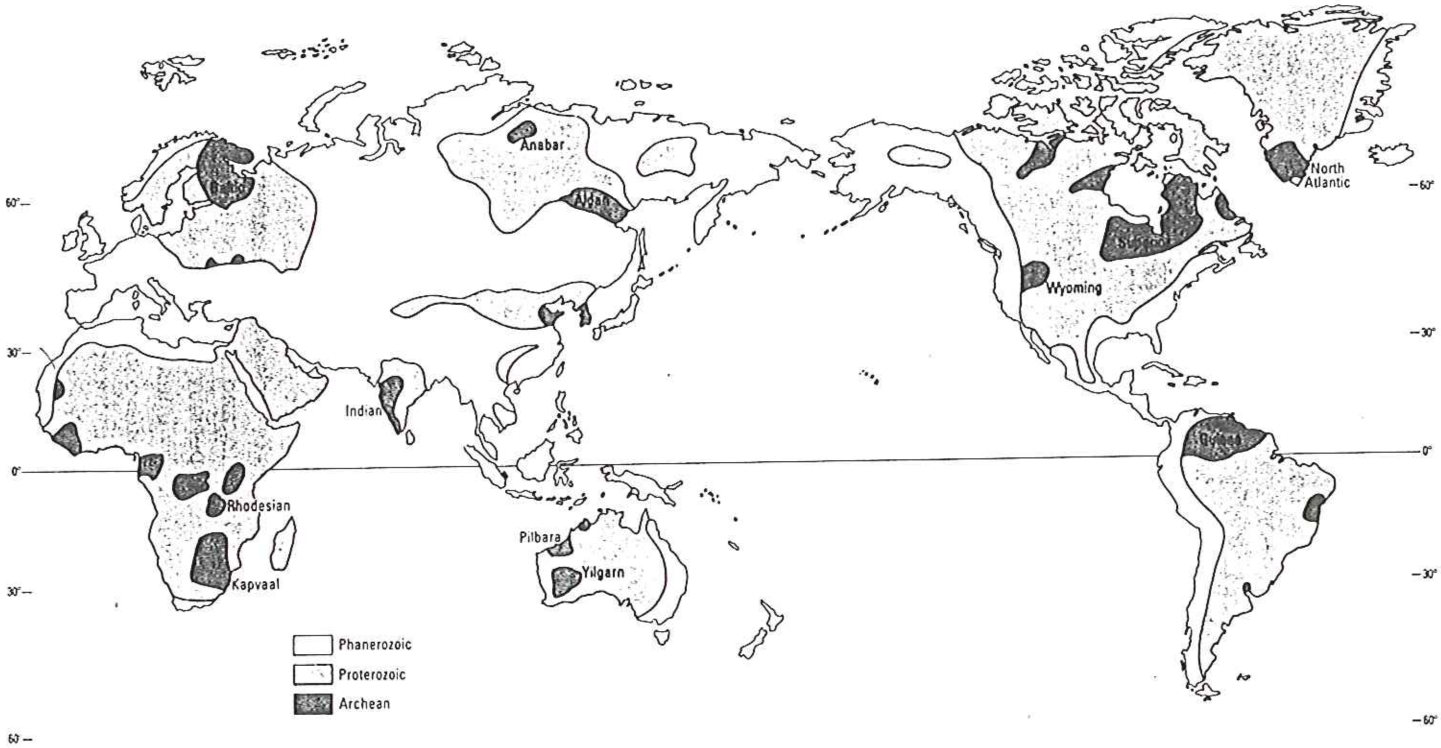


*Fig. 4.1.* Distribution of Archean and Proterozoic rocks. More than half of Antarctica (not shown) is also underlain by rocks of Precambrian age. (After various sources, including Condie, 1976, 1981, B.C. Burchfield, 1983, and Windley, 1984.)

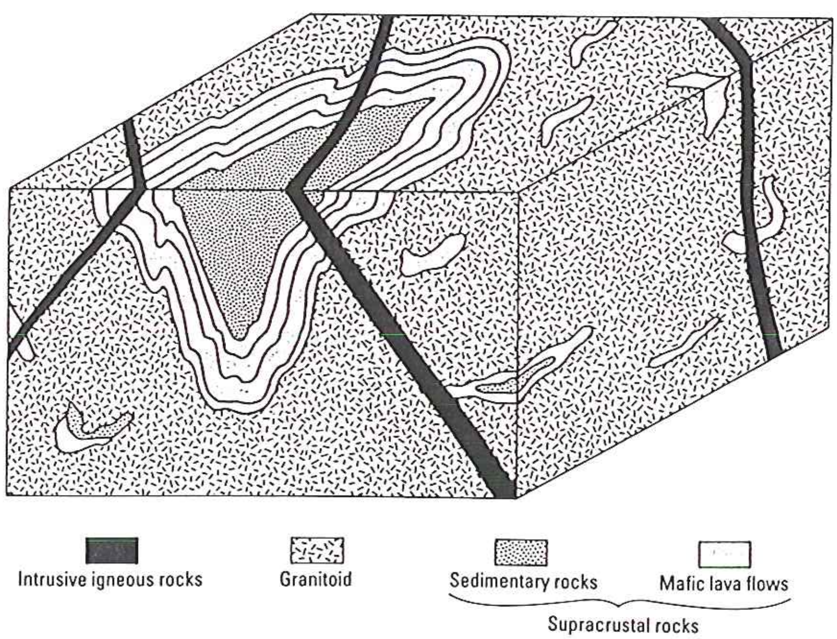


*Fig. 4.3.* Typical sequence in Archean terranes where the Earth's oldest rocks are found. Commonly, the oldest rocks, which occur as fragmented inclusions within the gneiss, are remnants of lava flows and of sedimentary rocks derived from still older rocks of which there is now no trace.

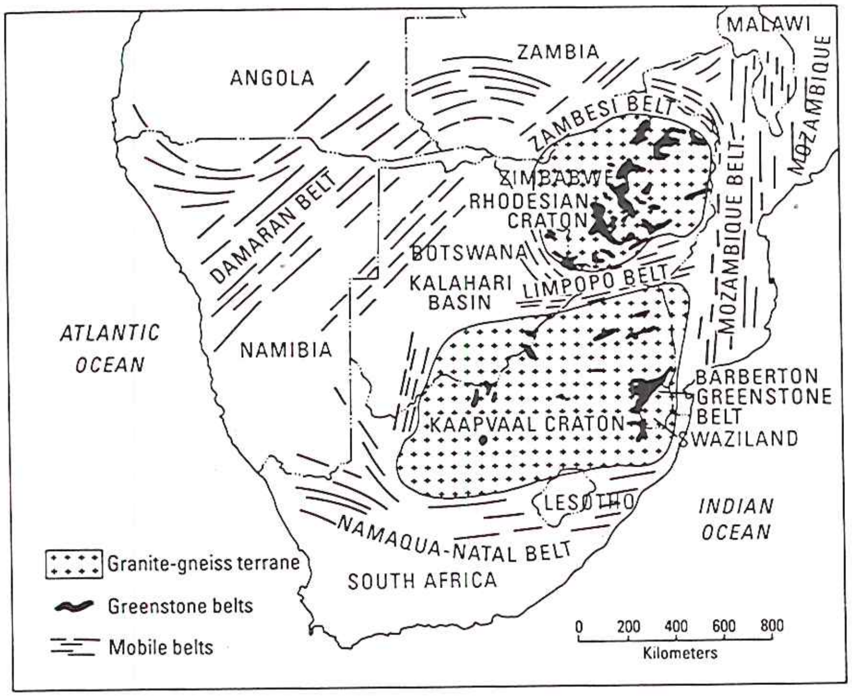


*Fig. 4.26.* The Archean cratons of southern Africa. The boundaries of the Kaapvaal and Rhodesian cratons are uncertain because large areas are concealed beneath younger rocks. (After R. Mason, 1973.)

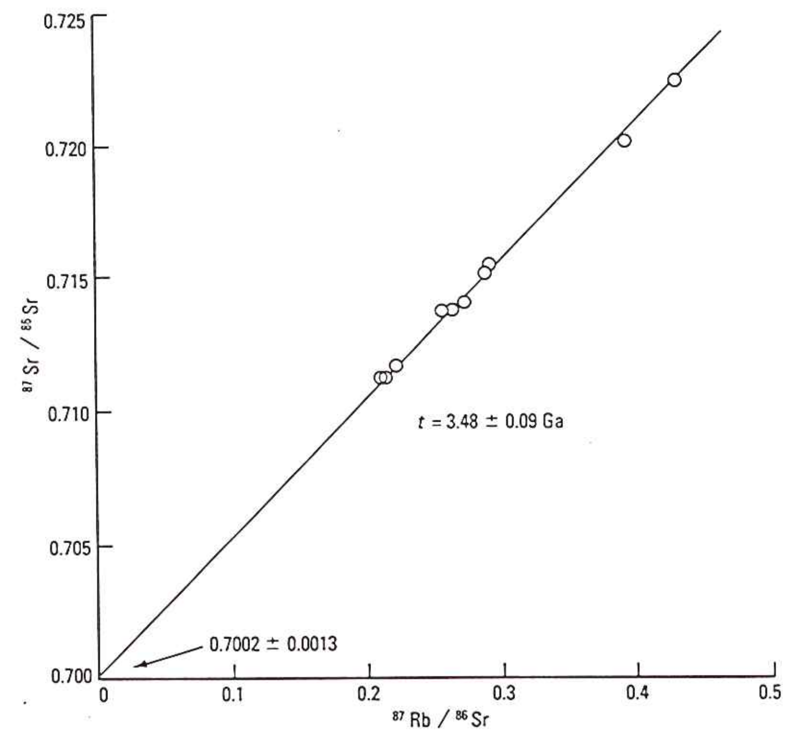


*Fig. 4.31.* Rb–Sr isochron for whole-rock samples from the Stolzburg Pluton, South Africa. (After Barton et al., 1983b.)

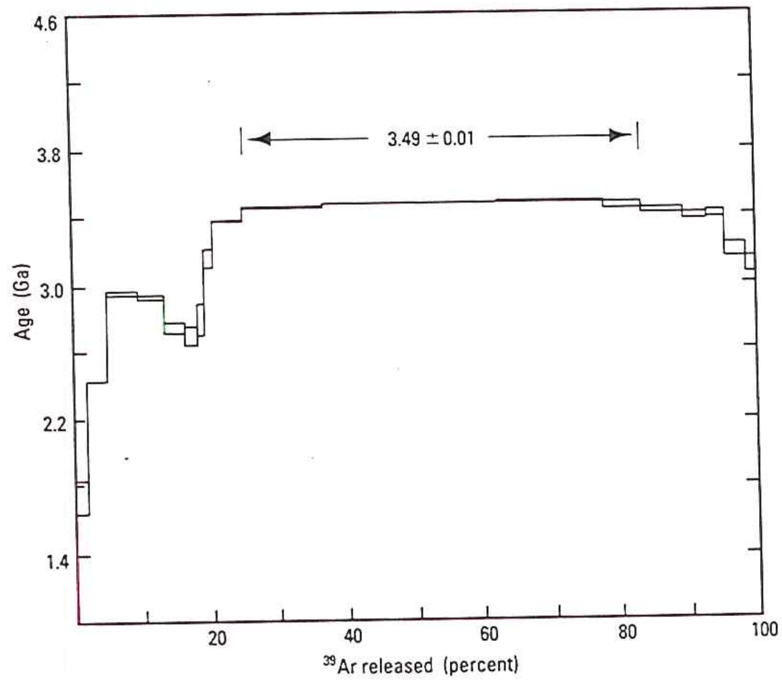


*Fig. 4.29.* $^{40}Ar/^{39}Ar$ age spectrum for a sample of komatiite from the Komati Formation, Onverwacht Group, Barberton Mountain Land, southern Africa. The vertical thickness of the boxes indicates the standard deviation of the value for each gas increment. Error in the plateau age indicates two standard deviations. (After M. Lopez Martinez et al., 1984.)

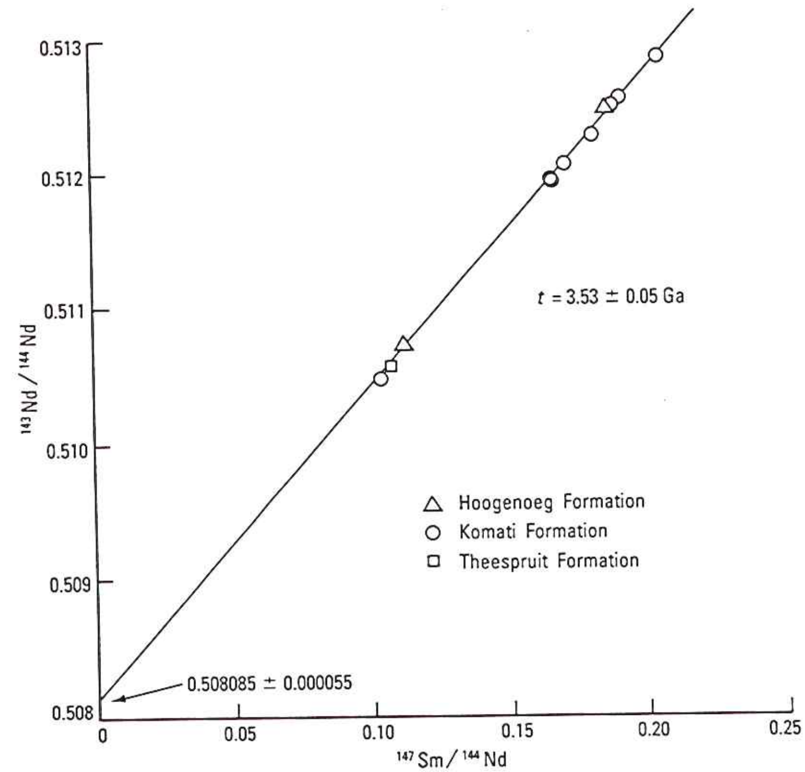


*Fig. 4.28.* Sm–Nd isochron diagram for volcanic rocks of the Komati and Theespruit formations, Onverwacht Group, Barberton Mountain Land, southern Africa. Two samples from the Hoogenoeg Formation are shown for comparison but were not included in the isochron calculation. (After Hamilton et al., 1979.)

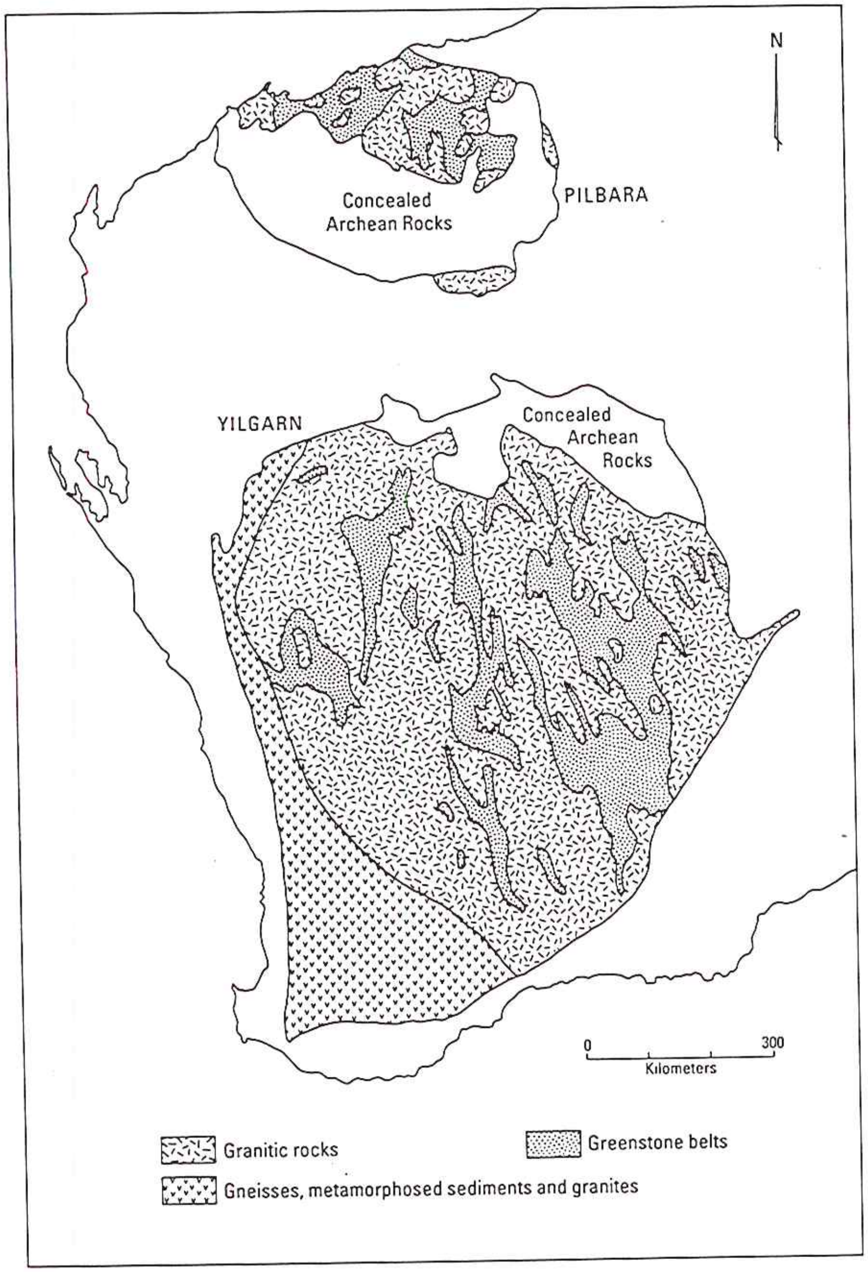


*Fig. 4.21.* Principal rock types of the Archean Pilbara and Yilgarn blocks, Western Australia. (After Rutland, 1981.)

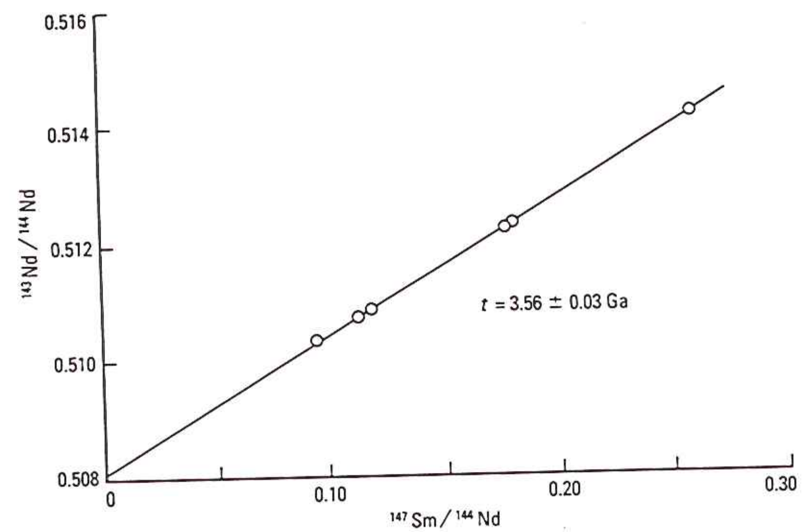


*Fig. 4.23.* Sm–Nd isochron diagram for samples of volcanic rocks from the North Star Basalt, the lowest formation in the Pilbara Supergroup, Pilbara Block, Western Australia. (After Hamilton et al., 1981.)

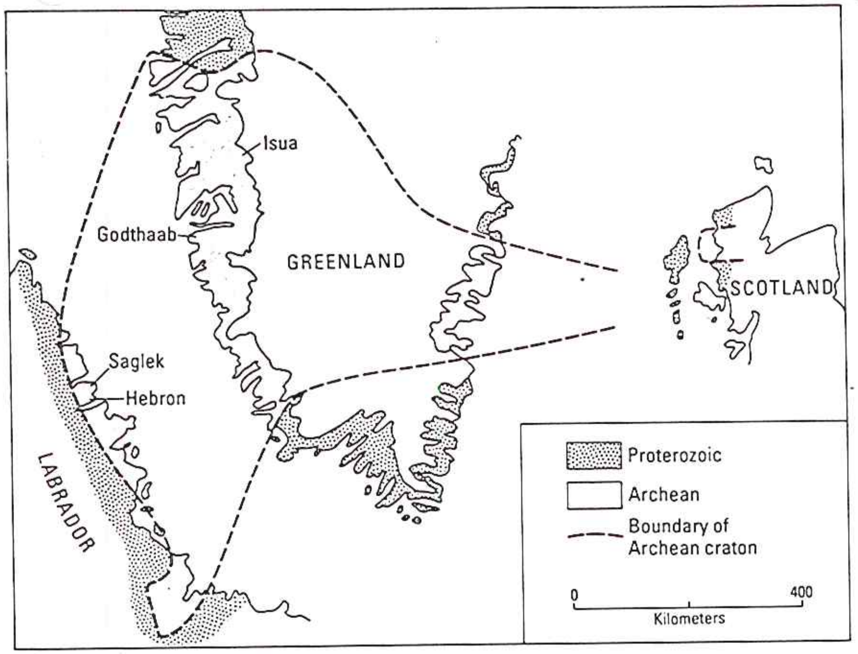


*Fig. 4.6.* The North Atlantic craton includes parts of Greenland, Labrador, Scotland, and Norway (not shown). The land masses, joined prior to about 200 Ma, are shown closer together than they are now. Precambrian rocks do not occur in the oceans that now divide the fragments of the craton. (After Bridgwater, Watson, and Windley, 1973.)

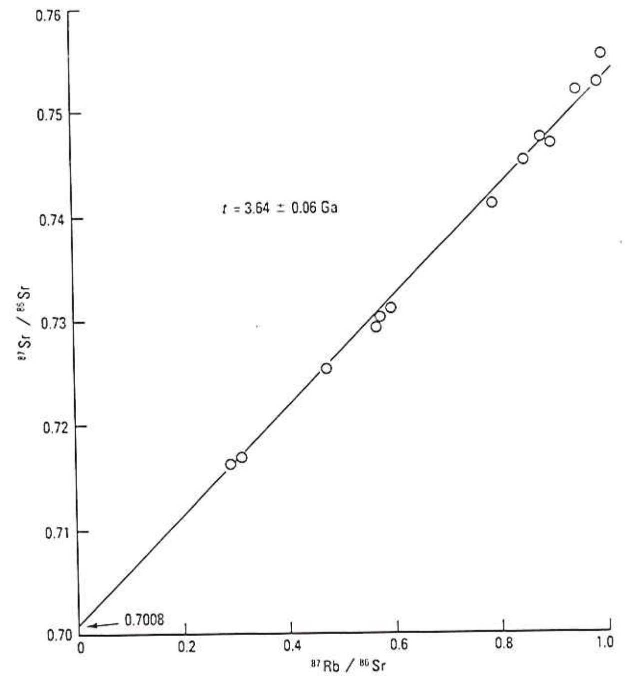


*Fig. 4.14.* Rb–Sr isochron diagram for samples of the Amitsoq gneisses at Isua. (After Moorbath et al., 1977a.)

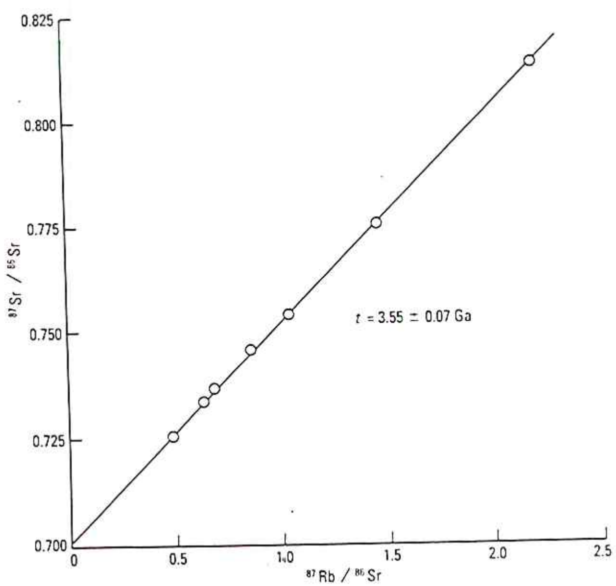


*Fig. 4.16.* Rb–Sr isochron diagram for samples of the Uivak gneisses near Saglek, eastern Labrador. (After Hurst et al., 1975.)

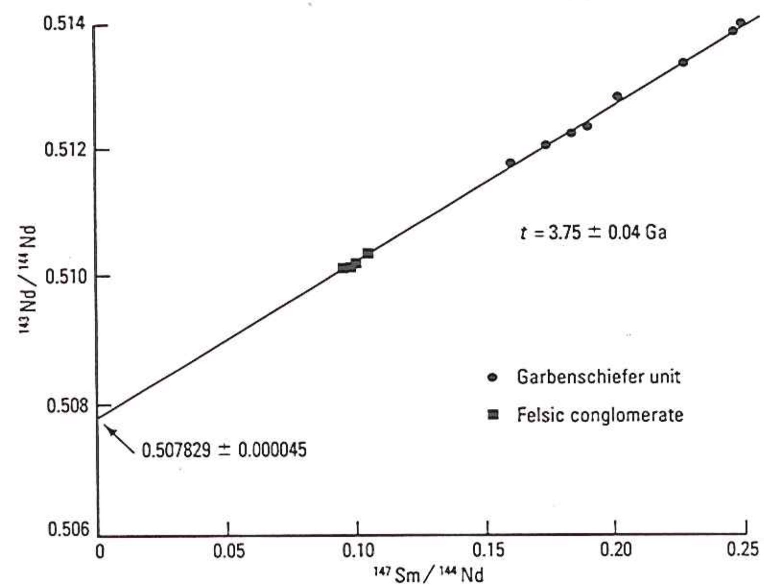


*Fig. 4.11.* Sm–Nd isochron diagram for samples from the garbenschiefer unit and the felsic conglomerate of the Isua supracrustals. (Data from Hamilton et al., 1978, 1983.)

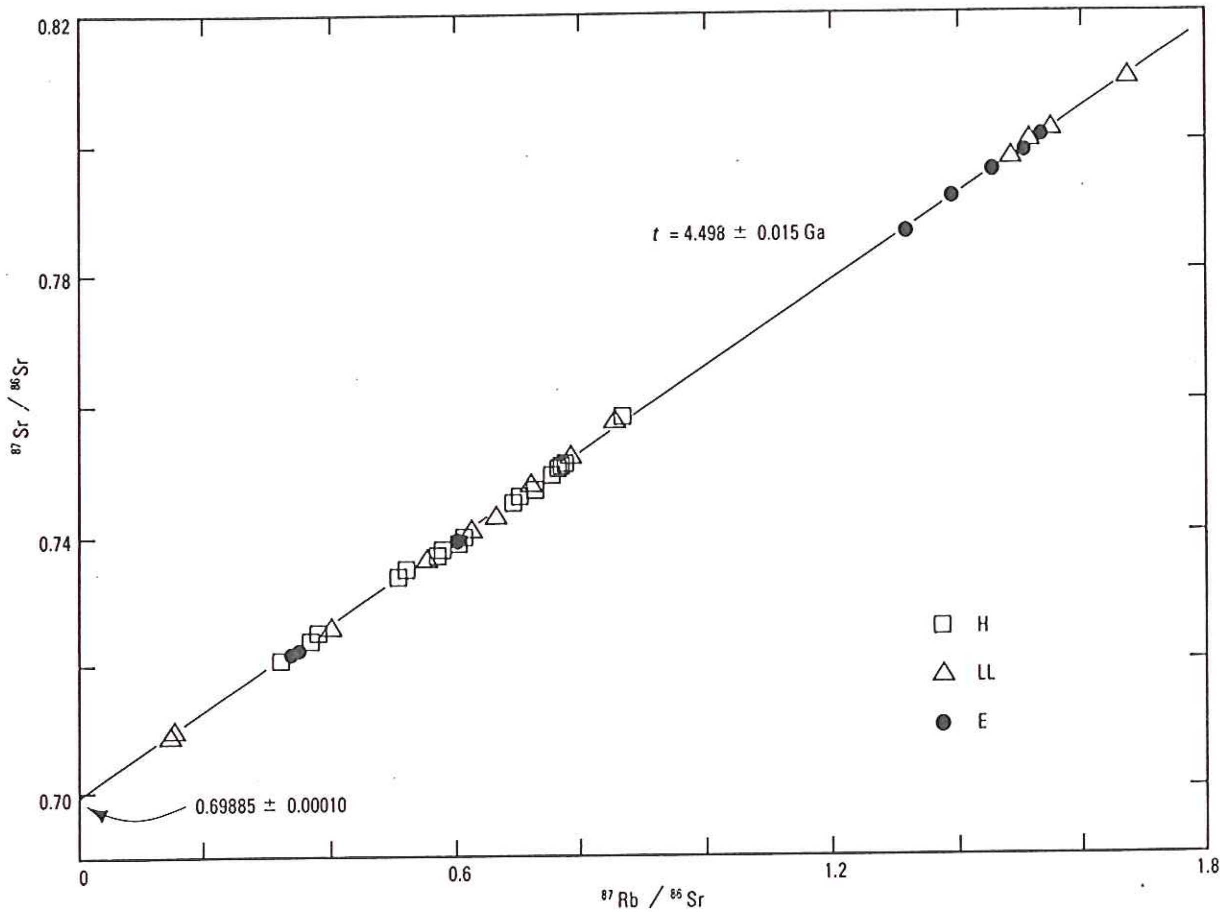


*Fig. 6.11.* Rb–Sr whole-rock isochron for 38 undisturbed H, LL, and E chondrites. (After Minster, Birck, and Allègre, 1982.)

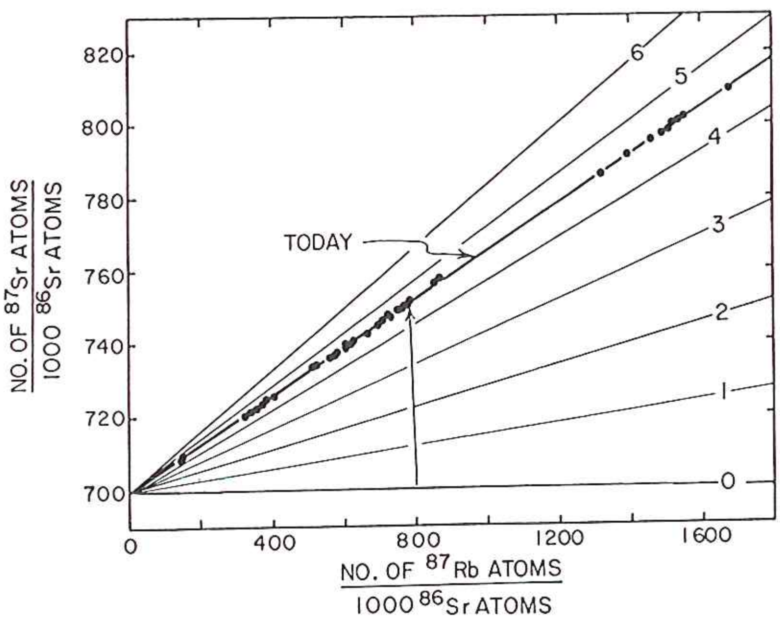


**Figure 4-2. Evolution of strontium isotope composition in minerals of differing rubidium contents:** The light lines on this diagram show the evolution with time (billions of years) of the $^{87}Sr$ and $^{87}Rb$ in meteorites. The measurements on mineral grains separated from chondritic meteorites tell us two things. First, they tell us that there were 700 $^{87}Sr$ atoms for each 1000 $^{86}Sr$ atoms in the strontium present in the solar nebula. Second, they tell us that these meteorites formed very close to 4.56 billion years ago. The former is derived from the intercept of the straight line that passes through the measured values. The latter is derived from the slope of the line passing through these points. Each grain followed a time trend parallel to that for the arrow shown on the diagram. At the time the solar system formed all the grains had compositions falling along the line marked zero, i.e., they had a range of $^{87}Rb$ to $^{86}Sr$ ratios, but all had 700 $^{87}Sr$ atoms per 1000 $^{86}Sr$ atoms. With time each grain increased in $^{87}Sr$ content (and decreased in $^{87}Rb$ content). This increase was in proportion to its $^{87}Rb$ content.

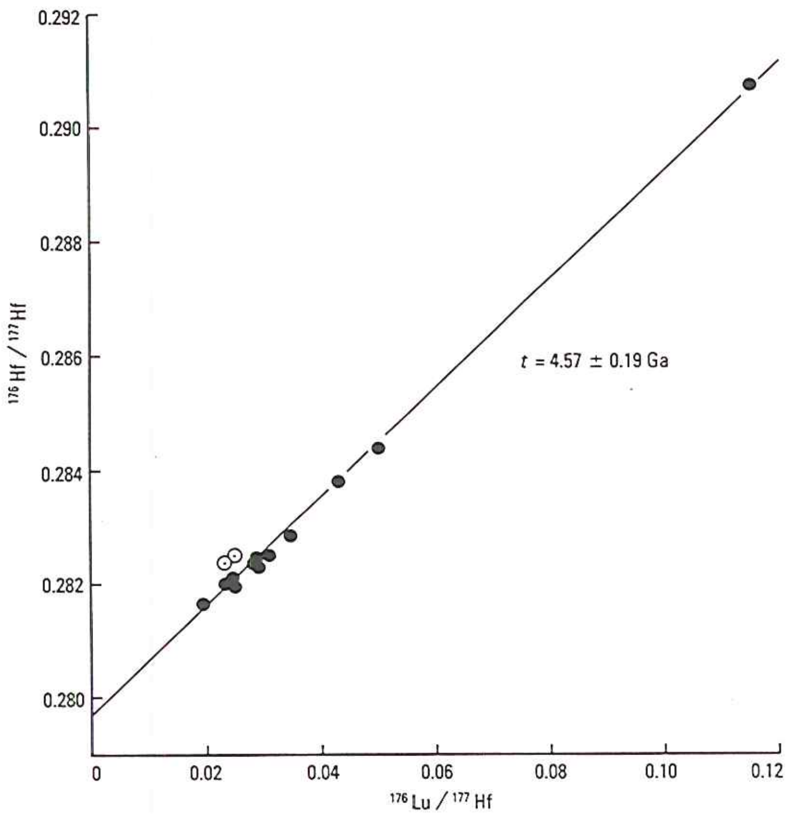


*Fig. 6.12.* Lu–Hf isochron for 13 eucrites (filled circles). The open circles are data for the antarctic eucrite ALHA77302, which do not fall on the isochron defined by the other eucrites. The age was calculated by using the experimentally determined value for the half-life of $^{176}Lu$ (Table 3.1). (After Patchett and Tatsumoto, 1980, with additional data from Tatsumoto, Unruh, and Patchett, 1981.)

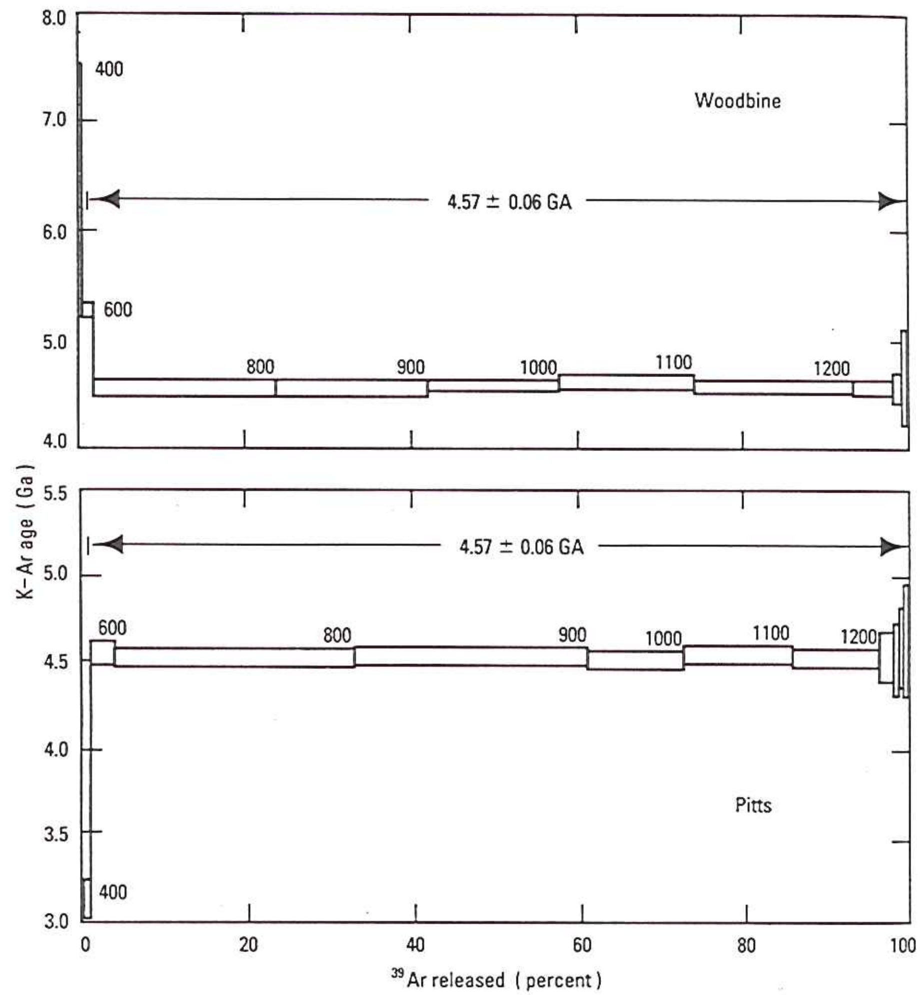


*Fig. 6.13.* $^{40}Ar/^{39}Ar$ age spectra for silicate inclusions in two iron meteorites. (After Niemeyer, 1979.)

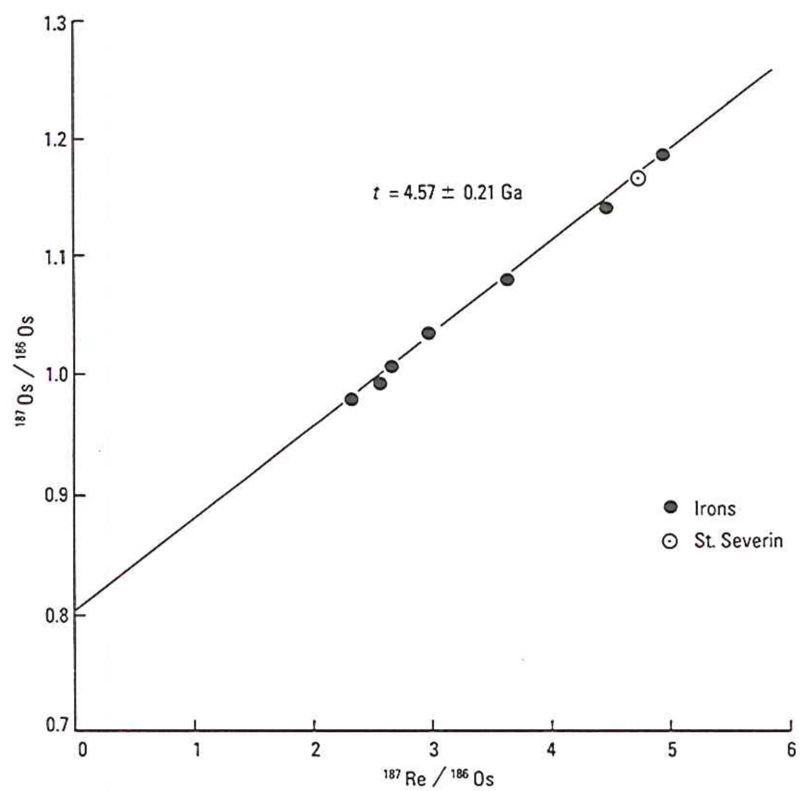


*Fig. 6.14.* Re–Os isochron for the metal phases of iron meteorites and the St. Severin LL chondrite. The age was calculated by using the experimentally determined value for the half-life of $^{187}Re$. (After Luck, Birck, and Allègre, 1980.)

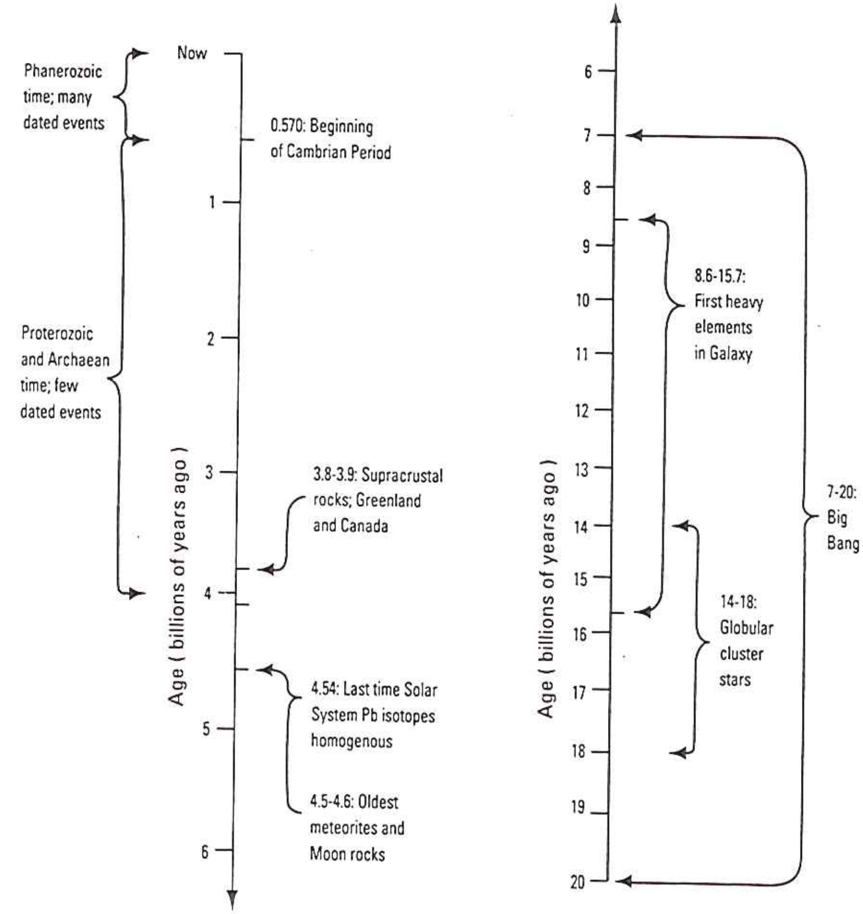


*Fig. 1.2.* Linear time scale of some important and datable events in the history of the Earth, the Solar System, the Galaxy, and the universe. The bases for the ages are discussed in chapters 4 through 8.

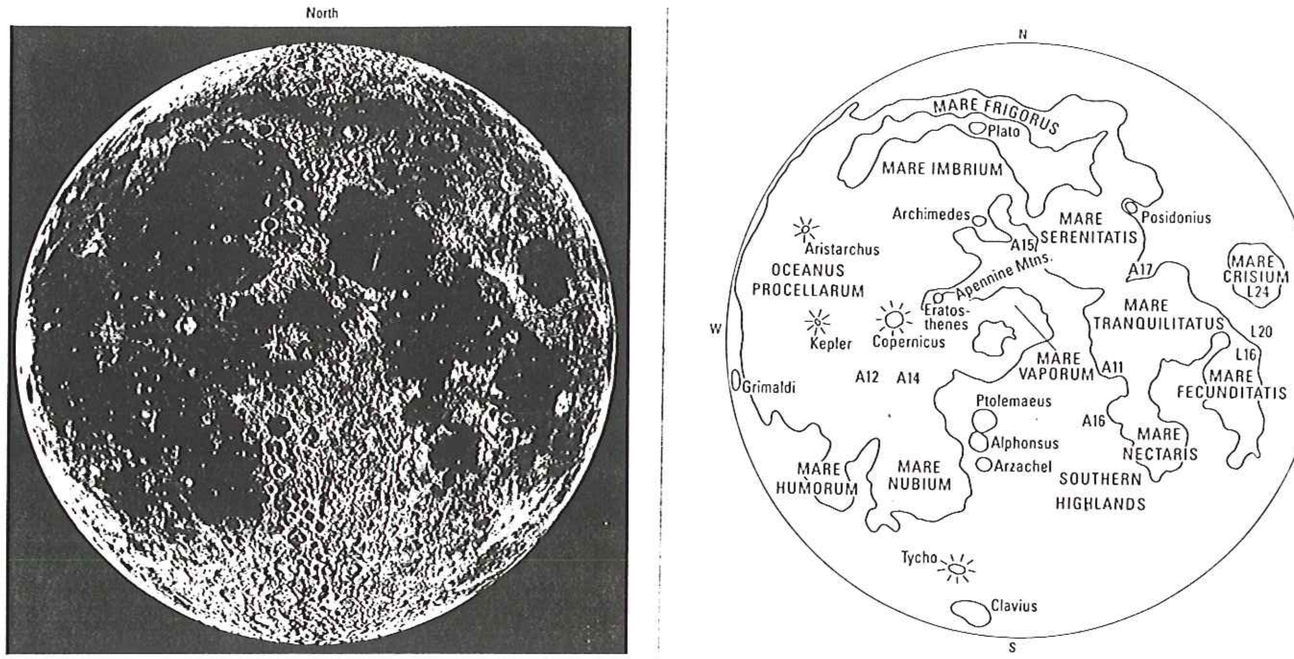


*Fig. 5.1.* The near side of the Moon, photograph (above) and diagram (opposite), showing some of the principal named features and the locations of the six Apollo (A) and three Luna (L) landing sites from which samples were returned to Earth. The dark smooth areas are maria; the brighter rugged areas are terrae (highlands). (Lick Observatory Photograph L-9, reproduced with permission.)

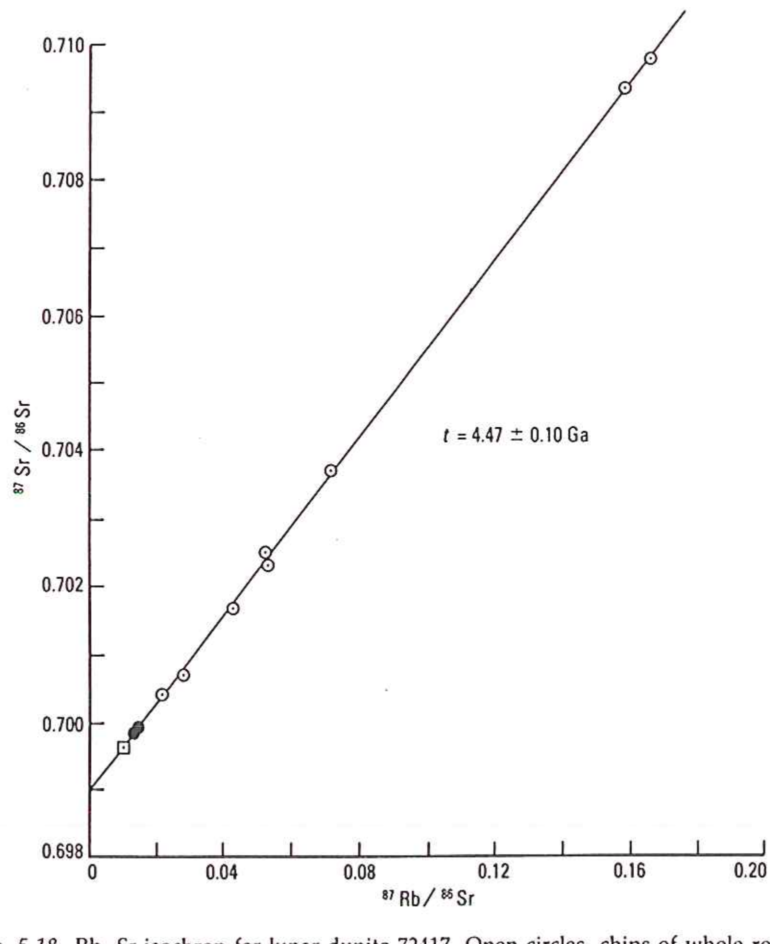


*Fig. 5.18.* Rb–Sr isochron for lunar dunite 72417. Open circles, chips of whole rock; filled circles, symplectites; square, olivine. All data were used in the isochron fit. (After Papanastassiou and Wasserburg, 1975.)